Dissociation of Sulfur Dioxide by Ultraviolet Multiphoton Absorption between 224 and 232 nm

Amitavikram A. Dixit

Department of Chemistry and Chemical Biology, Cornell University, Ithaca, New York 14853

Yuxiu Lei

Department of Chemistry and Chemical Physics Program, University of Puerto Rico, P.O. Box 23346, San Juan, Puerto Rico 00931-3346

Keon Woo Lee

Department of Chemistry and Chemical Biology, Cornell University, Ithaca, New York 14853

Edwin Quiñones*

Department of Chemistry and Chemical Physics Program, University of Puerto Rico, P.O. Box 23346, San Juan, Puerto Rico 00931-3346

Paul L. Houston*

Department of Chemistry and Chemical Biology, Cornell University, Ithaca, New York 14853

Received: October 14, 2004; In Final Form: December 13, 2004

Multiphoton excitation and dissociation of SO_2 have been investigated in the wavelength range from 224 to 232 nm. Strong evidence is found for two-photon excitation to the $\tilde{H}$ Rydberg state, followed by dissociation to SO + O and ionization of the SO product by absorption of a third photon. The two-photon excitation is resonantly enhanced via the $\tilde{C}\ ^1B_2$ intermediate state, and the two-photon yield spectrum thus bears a strong resemblance to the spectrum of this intermediate. Imaging of the $O(^3P_2)$, $S(^1D_2)$, and SO products suggests that, following dissociation of SO_2 from the $\tilde{H}$ state, SO is produced in the *A* and *B* electronic states. $S(^1D_2)$ is produced both from two-photon dissociation of SO_2 to give $S(^1D_2) + O_2$ and by single-photon dissociation of SO^+. In the former process, the O_2 is likely formed in all of its lowest three electronic states.

1. Introduction

Although the ground and lower excited states of SO_2 have been well studied,[1−6] highly excited states of SO_2 have received only limited attention. Golomb et al. recorded the VUV spectrum between 220 and 105 nm.[7] The diffuse absorption bands observed below 135 nm were assigned to transitions to Rydberg states.[7−9] Most studies on the Rydberg states of SO_2 have focused on the spectroscopy of the $\tilde{G}$ and the $\tilde{H}$ states. Typical techniques that have been used in these studies include fluorescence induced by excitation with xenon and hydrogen lines in the VUV region,[8,10,11] synchrotron radiation spectroscopy,[12] electron energy loss spectroscopy[13−15] and nonresonant multiphoton ionization.[16,17] Lalo et al. have investigated the gas-phase photochemistry at excitation wavelengths of 116.5, 123.6, and 147 nm.[18,19]

The VUV region can also be accessed by absorption of two photons in the UV region. Although two-photon absorption and dissociation in the 248−311 nm range, which includes excitation of the $\tilde{G}$ Rydberg state at 248 nm, has been studied by many groups,[20−23] a similar two-photon study of the $\tilde{H}$ Rydberg state has not yet been reported. The $\tilde{H}$ Rydberg state has been studied in one-photon absorption by Suto et al., who used synchrotron radiation in the 106−133 nm range to measure photoabsorption and fluorescence cross sections.[12] The observed fluorescence was attributed to the SO radiation from the $A\ ^3\Pi$ and the $B\ ^3\Sigma^-$ electronic states. The fluorescence yield as a function of excitation wavelength was nearly identical to the absorption spectrum. In the present study, ultraviolet multiphoton dissociation of SO_2, following multiphoton absorption in the range 224−230 nm, was studied. The velocity-mapped ion imaging technique was used to understand the dynamics of the photodissociation process.[24]

2. Experimental Section

Experiments were performed both at Cornell University and at the University of Puerto Rico, Rio Piedras. In the Cornell experiments, a 10% SO_2/Ar mixture was expanded through a pulsed piezoelectric nozzle at a backing pressure of 2 psig. The molecular beam was collimated by a 500 μm diameter skimmer mounted about 0.5−1.0 cm from the nozzle orifice. The dissociation and probe lasers propagated in opposite directions. The molecular beam was crossed downstream by the laser beams at a right angle. In this experiment, SO_2 was dissociated in the wavelength region from 224 to 232 nm. The dissociation laser was focused with a 10 in. focal length lens. The dissociation laser produces an ion signal corresponding to the SO fragment. Both the SO + O and S + O_2 channels were studied by detecting the $O(^3P_2)$ or $S(^1D_2)$ atom from dissociation of SO_2 using

10.1021/jp0453010 CCC: $30.25
Published on Web 02/11/2005

resonance enhanced multiphoton ionization. Velocity mapped ion imaging was used, and the ions were imaged onto a position sensitive detector comprising a double-chevron microchannel plate (MCP) assembly (Galileo) coupled to a fast phosphor screen. The image on the detector was recorded by a 640 × 480 pixel CCD camera (Xybion). Both the MCP and the camera were electronically gated on the mass of interest in the time-of-flight spectrum to record signal corresponding to the particular fragment. The magnification factor of the electrostatic lens was measured by dissociation of O_2 and detection of $O(^3P_2)$ fragment at the REMPI wavelength of 225.65 nm in a single-color experiment. Both single-color (only dissociation laser) and two-color experiments (dissociation and probe lasers) were carried out. In the single-color experiment, the SO fragment was imaged, because an ion signal corresponding to the SO fragment was observed in the mass spectrum. In the two-color experiment, the O or the S fragment was imaged. Signal levels were kept below 300 ions per frame to ensure accurate ion counting and centroiding.

The ion signals for S^+ and SO^+ were also recorded at the University of Puerto Rico, where a homemade Wiley−McLaren linear time-of-flight spectrometer (TOF) was employed. A 1 in. diameter microchannel plate (Hamamatsu) mounted on a Teflon base was used to detect the ions, and the distance between the ionization region and the detector was 0.25 m. Commercial SO_2 (AGA Products) was expanded from a pulsed valve with nozzle orifice 0.1 mm. The optimum expansion condition for acquiring the action spectra was pure SO_2 at a backing pressure 150 Torr. The frequency-doubled output of an excimer-pumped dye laser (Lambda Physik) induced the multiphoton processes in SO_2. The mass distributions were displayed on a 300 MHz oscilloscope (LeCroy 9361C). Action spectral data acquisition was performed by a personal computer (Macintosh G4) linked to a boxcar system and other devices through a Labview GPIB interface (National Instruments). The positions of the Xe^+ produced by a (2+1) ionization via $(5p^5)P_{3/2}°(7p)[5/2]_{J=2}$ at 88 352.20 cm^{-1} and $(5p^5)P_{3/2}(7p)[3/2]_{J=2}$ at 88 687.020 cm^{-1} were used to calibrate the laser frequency.

3. Results and Discussion

3.1. Single-Color Yield Spectrum of SO^+ and S^+. The yield spectrum for the SO fragment was obtained by photolyzing a 1% SO_2/Ar mixture in the wavelength region from 224 to 232 nm using a dissociation laser focused with a 10" focal length lens. The time-of-flight mass spectra showed peaks corresponding to SO^+ and S^+ ions. The ion signal from SO^+ was then monitored while the dissociation laser was scanned. The yield spectrum for SO^+ fragment in the 224−232 nm wavelength range showed distinct bands corresponding to progressions for the C $^1B_2$ electronic intermediate state. Figure 1 shows the ion yields from both S^+ and SO^+ as a function of the dissociation wavelength along with the assignments for the C $^1B_2$ electronic intermediate state. The SO^+ fragment was then detected in a single-color experiment and an energy dependence study was performed with the laser tuned to one of the peaks in the band observed at 231.7 nm. A plot of the logarithm of the total SO^+ ion signal versus the logarithm of the energy was linear with a slope of 3.1, indicating a multiphoton pathway.

3.2. Origin of SO^+ and S^+. At least two possible pathways should be considered in the multiphoton excitation of SO_2 in the 224−232 nm wavelength range, either dissociation from a state of SO_2^+ reached by absorption of three photons or dissociation from an excited state of SO_2 (perhaps the $\tilde{H}$ Rydberg state) reached by absorption of two photons followed by nonresonant ionization of the product S or SO.

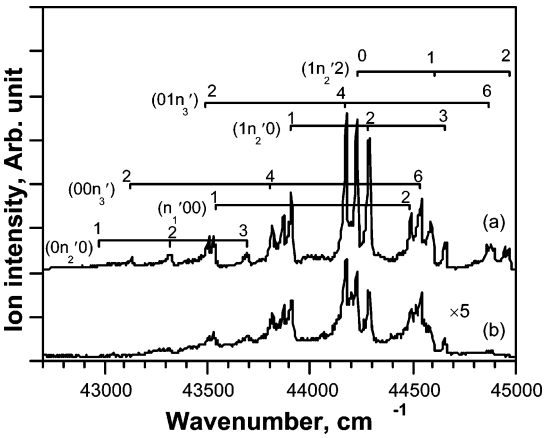

Figure 1. Yield spectra from multiphoton dissociation of SO_2 in the range 42 700−45 000 cm^{-1}: (a) SO^+; (b) S^+.

The ionization threshold of SO_2 is 12.3 eV. The energy of three photons in the 224−232 nm range (16.03−16.60 eV) is greater than the ionization threshold of SO_2, so it might be plausible that the observed SO^+ signal arises from fragmentation of the parent ion SO_2^+. However, SO_2^+ was not observed in the time-of-flight mass spectrum over the 224−232 nm region investigated in this study. Weiss et al. have studied fragmentation of SO_2^+ prepared in state-selected vibrational levels in the energy range of 15.844 to 16.674 eV.[25] The threshold photoelectron-coincident photoion mass spectra in the 16.189 to 16.441 eV energy range, which can be accessed by three photons in the current experiment, show peaks corresponding to SO_2^+. The time-of-flight for the SO_2^+ ions was around 35 μs, indicating that the lifetime of the SO_2^+ ions must at least be 35 μs. On the basis of the voltages in the electrostatic lens in the ion-imaging apparatus, the time-of-flight for SO_2^+ in our experiment is calculated to be less than 15 μs. Thus, the absence of an SO_2^+ ion peak in the time-of-flight spectrum indicates that absorption of three UV photons in the 224−232 nm wavelength range leading to formation of SO_2^+ and subsequent fragmentation is not a dissociation pathway.

An alternative explanation to account for the observation of SO^+ is that it arises from two-photon dissociation of SO_2 to give SO + O near a total energy of 11 eV, followed by nonresonant ionization of SO. (S^+ might then be produced by further absorption by SO^+ followed by dissociation.) There is certainly support in the literature for dissociation of SO_2 in this energy region. First, Dujardin and Leach used a photoion-fluorescence photon coincidence technique to study radiative and dissociative processes in SO_2 excited by line photoexcitation sources in the range 10.2−21.2 eV.[26] With the Ne(I) excitation at 16.8 eV, the main emission was found to be from neutral species. Comparison with the emission spectra at H(I) (10.2 eV) and Ar(I) (11.62 eV) excitation energies, which are below the ionization threshold for SO_2, revealed that the emission was from neutral SO ($A\ ^3\Pi$) and SO ($B\ ^3\Sigma^-$) electronic states. It is possible that excited Rydberg levels of neutral SO_2 are accessed by the Ne(I) excitation. Second, Suto et al. observed the fluorescence yields from photodissociation of SO_2 using synchrotron radiation in the 106−133 nm range, which accesses the $\tilde{H}$ Rydberg state of SO_2.[12] The fluorescence yield indicated that both SO($A\ ^3\Pi$) and SO($B\ ^3\Sigma^-$) are produced in the dissociation of the $\tilde{H}$ Rydberg state. It thus seems likely that two-photon excitation of SO_2 will produce SO electronic states that are sufficiently excited so as to be ionized by absorption

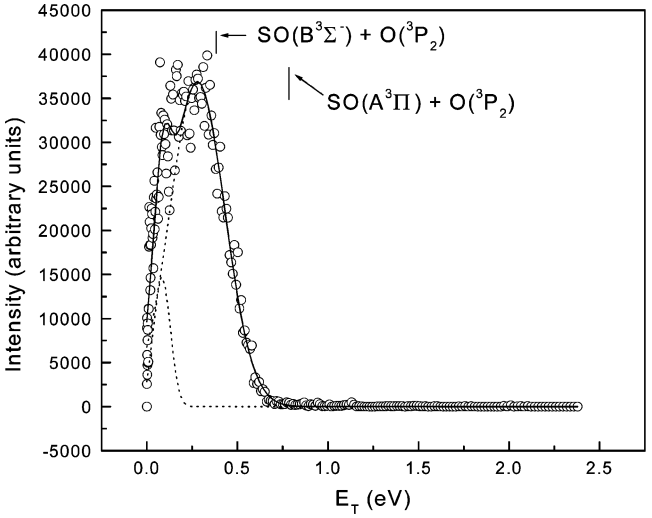

Figure 2. Total translational energy distribution obtained for dissociation via intermediate (0, 0, 6) band of the C^1B_2 state by analyzing the image for SO.

of a third 224−232 nm photon. The SO($A\ ^3\Pi$) state can just be ionized with a photon at 5.5 eV.

The SO^+ produced in our one-color experiment was imaged, and the image analyzed to obtain the energy distribution for SO^+ produced in excitation through the (0, 0, 6) band at 224.457 nm (5.52 eV). The results are shown in Figure 2, which also provides the energetic thresholds for the SO($A\ ^3\Pi$) + O(^{3}P) and SO($B\ ^3\Sigma^-$) + O(^{3}P) channels assuming two-photon excitation. Note that the energy distribution does not extend beyond the energetic threshold for the SO($A\ ^3\Pi$) + O(^{3}P) channel; most of the intensity appears to be associated with the SO($B\ ^3\Sigma^-$) + O(^{3}P) channel. The ground vibrational state in the $A\ ^3\Pi$ electronic state is 5.54 eV below the ionization threshold for the SO radical. Thus, although vibrationally excited SO radicals in the $A\ ^3\Pi$ electronic state might be ionized by absorption of one photon at 224.457 nm (5.52 eV), electronic states of SO lower in energy than the $A\ ^3\Pi$ state cannot be ionized by absorption of one photon. Nonresonant two-photon ionization of electronic states below the $A\ ^3\Pi$ state is unlikely.

Further qualitative evidence for this interpretation comes from a two-color experiment in which the two-photon excitation laser is tuned to an SO_2 $\tilde{C}$ state intermediate resonance and a 355 nm laser is fired following a delay of 0−500 ns. A second SO^+ peak is observed at the corresponding delay, due to the fact that the strong 355 nm laser can more efficiently ionize SO(A) or SO(X) in a two-photon process whereas predominantly SO(B) is ionized by the tunable laser in a one-photon process.

The energy distribution in Figure 2 was analyzed by fitting it with two Gaussians corresponding to the generation of the SO($A\ ^3\Pi$) + O(^{3}P) and SO($B\ ^3\Sigma^-$) + O(^{3}P). The fit suggests significant vibrational excitation in the SO fragments. Because the ionization efficiency of SO($A\ ^3\Pi$) depends on vibrational level, it is not possible to quantify relative yields for the two channels. The fact that the energy distribution does not extend beyond the energetic threshold for the SO($A\ ^3\Pi$) + O(^{3}P) channel lends further support to the thesis that SO and O products are produced by two-photon dissociation of SO_2 .

3.3. O(^{3}P) Image. Oxygen atoms were imaged in a single-color experiment at 225.65 nm. The resulting raw image is shown in Figure 3. At this wavelength, the oxygen fragment from the dissociation is resonantly ionized. The energy distribution obtained from the image is shown in Figure 4.

The energy distribution in this figure is difficult to rationalize if the dissociation follows a three-photon pathway. The maximum allowed total translational energy for the SO ($A\ ^3\Pi$) + O (^{3}P) channel in this case would be 6.18 eV. The maximum total translational energy observed experimentally is close to 2.25 eV. This would imply that the SO fragment in the $A\ ^3\Pi$ state has a vibrational excitation of at least 3.93 eV. Elks and Western studied the $A\ ^3\Pi - X\ ^3\Sigma^-$ transition in SO radical by laser induced fluorescence and resonant multiphoton ionization.[27] Their study indicates that the dissociation limit for the $A\ ^3\Pi$ state of SO lies between $v' = 13$ and $v' = 14$, at about 0.5 eV above the lowest vibrational state. Thus, the minimum vibrational excitation of 3.93 eV in the $A\ ^3\Pi$ state of SO, implied by the three-photon pathway, is far higher than the dissociation limit for the $A\ ^3\Pi$ electronic state. Consequently, if SO($A\ ^3\Pi$) is a major product, as suggested from fluorescence studies, it is unlikely that the dissociation is the result of a three-photon pathway.

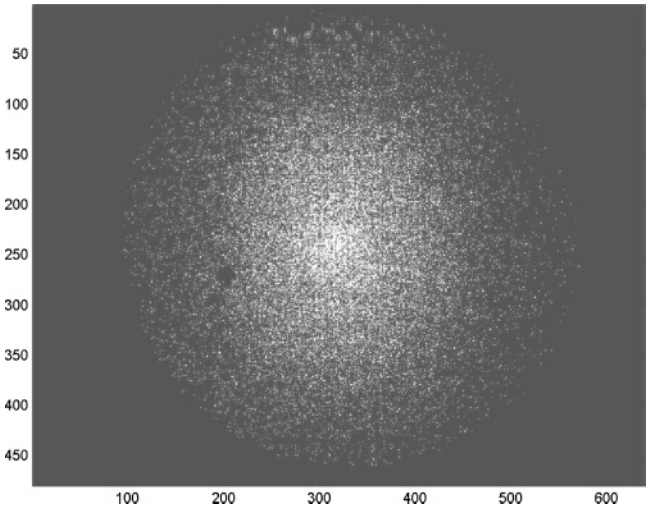

Figure 3. Raw image of O(^{3}P$_2$) from two-photon dissociation of SO_2.

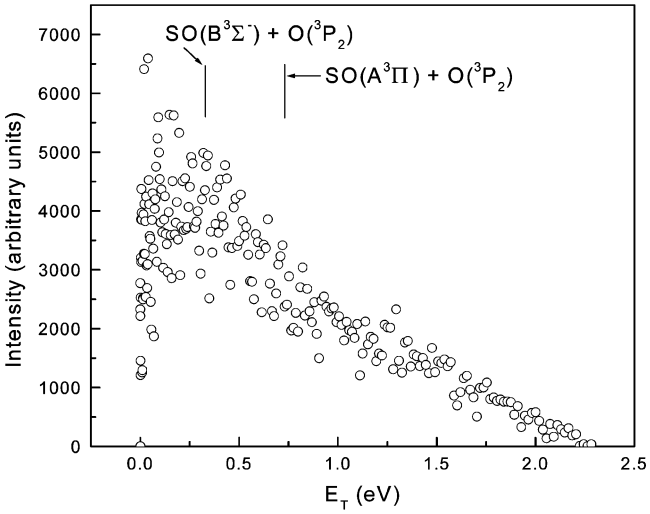

Figure 4. Total translational energy distribution at 225.65 nm obtained by imaging O(^{3}P$_2$).

Alternatively, a two-photon process seems likely. The energetic thresholds for SO($A\ ^3\Pi$) + O(^{3}P) and SO($B\ ^3\Sigma^-$) + O(^{3}P) channels, based on the two-photon dissociation pathway, are shown in Figure 4. Although some intensity in the total translational energy distribution lies above the energetic threshold for the SO($A\ ^3\Pi$) + O(^{3}P) channel, it is possible that it is due to contributions from channels involving the coincident production of O(^{3}P) with electronic states of SO that are lower in energy than SO($A\ ^3\Pi$). The lowest two singlet electronic

states, SO($a\ ^1\Delta$) and SO($b\ ^1\Sigma^+$), if produced in coincidence with the O(^{3}P) fragment, would give limits on the maximum total translational energy of 4.99 and 4.18 eV respectively. If the channels corresponding to generation of the lowest two singlet electronic states of SO are present then a minimum vibrational excitation of 2.74 and 1.93 eV in the SO($a\ ^1\Delta$) and SO($b\ ^1\Sigma^+$) electronic states, respectively, is calculated. The well depths for the SO($a\ ^1\Delta$) and SO($b\ ^1\Sigma^+$), calculated from RKR potential energy curves presented elsewhere,[28] are 4.8 and 4.18 eV respectively. Hence, it is possible to observe the calculated vibrational excitation in the SO($a\ ^1\Delta$) and SO($b\ ^1\Sigma^+$) fragments. On the basis of the vibrational frequencies reported by Ornellas et al.,[29] the minimum vibrational energy corresponds to $v = 20$ and $v = 14$ in the SO($a\ ^1\Delta$) and the SO($b\ ^1\Sigma^+$) fragments, respectively. In the two-photon dissociation of SO_2 between 248 and 291 nm, the SO fragment in the $a\ ^1\Delta$ and $b\ ^1\Sigma^+$ electronic states was observed to have high vibrational excitation.[30] Effenhauser et al. have studied the two-photon dissociation of SO_2 at 248 and 308 nm.[20] The three internal energy thresholds observed experimentally at 28500, 29100 and 30400 cm^{-1} were assigned respectively to SO($c\ ^1\Sigma^-$), SO($A'\ ^3\Delta$), and SO($A''\ ^3\Sigma^+$) states generated in coincidence with O(^{3}P). These channels are energetically feasible on the basis of the experimental total translational energy distribution shown in Figure 4. The maximum translational energy threshold for the SO($c\ ^1\Sigma^-$) + O(^{3}P) channel at 225.65 nm is at 1.946 eV. This is close to the maximum observed total translational energy in Figure 4.

3.4. S(^{1}D) Image. Quantitative information on the internal energy distribution of the O_2 fragment in different electronic states can be derived if the S fragment from the S + O_2 channel is resonantly ionized and imaged. In a two-color experiment, a 10% SO_2/Ar mixture was dissociated at 229.647 nm via the (1, 0, 0) intermediate band, and S(^{1}D$_2$) was resonantly ionized at 288.22 nm by a 2+1 ionization scheme. The ion signal from S^+ was imaged by gating the detector on the mass of sulfur. The image is corrected for individual backgrounds from the dissociation and the probe lasers. We discuss these briefly before describing the image.

The dissociation wavelength contributes to the S^+ signal, and it was minimized by defocusing the dissociation laser. The likely source for the observed S^+ signal is from the dissociation of SO^+ by absorption of one photon. On the basis of the heats of formation for SO^+ and S^+ calculated by Liston et al.,[31] photon of 5.56 eV energy can dissociate SO^+. In the current investigation, identical peaks were observed in the ion yield spectra for both S^+ and SO^+, as shown in Figure 1. This observation is consistent with dissociation of SO^+ as the origin of S^+.

The dissociation of SO_2 by two-photon absorption at 288.22 nm also contributes to a background in the two-color experiment.[32] The image was thus corrected for the backgrounds from both the dissociation and the probe lasers. The energy distribution extracted from the corrected image is shown in Figure 5. On the basis of energy and momentum conservation and the dissociation threshold for the S + O_2 channel (5.9 eV), the maximum energy distributed in O_2 is 3.75 eV, consistent with S(^{1}D$_2$) generated in coincidence with O_2 in the $X\ ^3\Sigma$ (0 eV), $a\ ^1\Delta$ (1 eV), and $b\ ^1\Sigma$ (1.6 eV) electronic states.

3.5. Intensity Dependence. The translational energy distributions obtained in the current investigation support the dissociation mechanism via the $\tilde{H}$ Rydberg state. To confirm the interpretation presented earlier, the dependences of the ion yields for S^+ and SO^+ were studied as a function of the laser intensity. A model for the dissociation process based on a rate equations approach was used, and the equations derived for the concentration of the ion signals explains the experimentally observed dependencies. The model is schematically depicted in Figure 6. Figure 6a shows the scheme for generation of SO^+ and S^+ via a two-photon excited-state denoted as SO_2*. The one-photon intermediate resonance is assumed to be saturated and the absorption cross-section to reach the two-photon dissociative state is denoted by σ_1. The absorption of a third photon could occur with a cross-section σ_2 from the two-photon excited state. The rate equations for the two-photon dissociation model are

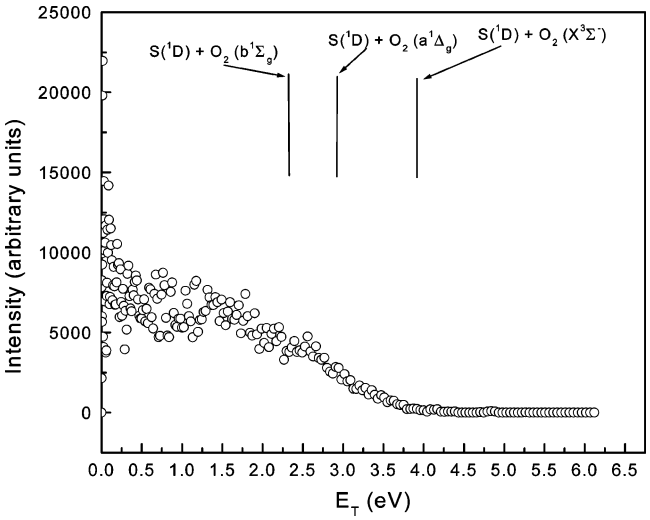

Figure 5. Total translational energy distribution obtained for dissociation via intermediate (1, 0, 0) band of the $\tilde{C}^1B_2$ state by analyzing the image for S(^{1}D$_2$).

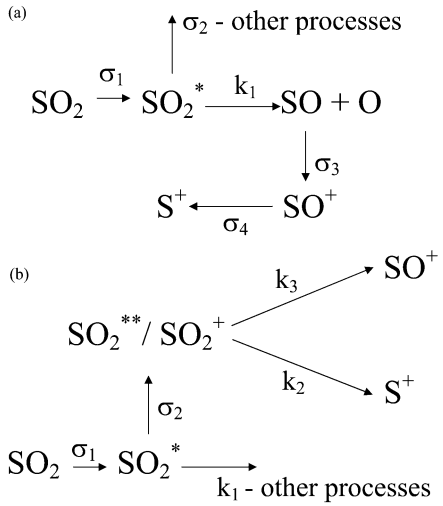

Figure 6. Models for rate equations approach: (a) two-photon scheme; (b) three-photon scheme

$$\frac{d[SO_2]}{dt} = -\sigma_1 I[SO_2]$$

$$\frac{d[SO_2^*]}{dt} = -\sigma_2 I[SO_2^*] - k_1[SO_2^*] + \sigma_1 I[SO_2]$$

$$\frac{d[SO]}{dt} = k_1[SO_2^*] - \sigma_3 I[SO]$$

$$\frac{d[SO^+]}{dt} = \sigma_3 I[SO] - \sigma_4 I[SO^+]$$

$$\frac{d[S^+]}{dt} = \sigma_4 I[SO^+] \qquad (1)$$

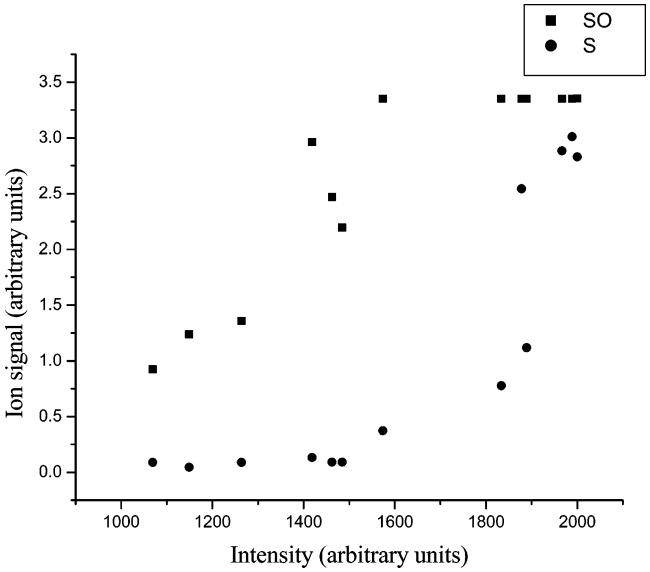

Figure 7. Ion signals from SO^+ and S^+ as a function of the laser intensity at the most intense band in the action spectrum.

The steady-state approximation was made for SO_2* whereas the other equations were derived exactly. The concentrations for SO^+ and S^+ are then given by the expressions

$$[SO^+] = A\left[\left(\frac{e^{-\sigma_4 It} - e^{-\sigma_3 It}}{\sigma_3 - \sigma_4}\right) - \left(\frac{e^{-\sigma_4 It} - e^{-\sigma_1 It}}{\sigma_1 - \sigma_4}\right)\right]$$

$$[S^+] = \sigma_4 A\left[\left(\frac{1 - e^{-\sigma_4 It}}{\sigma_4(\sigma_3 - \sigma_4)}\right) - \left(\frac{1 - e^{-\sigma_3 It}}{\sigma_3(\sigma_3 - \sigma_4)}\right) - \left(\frac{1 - e^{-\sigma_4 It}}{\sigma_4(\sigma_1 - \sigma_4)}\right) + \left(\frac{1 - e^{-\sigma_1 It}}{\sigma_1(\sigma_1 - \sigma_4)}\right)\right] \quad (2)$$

where

$$A = \frac{\sigma_3 k_1 \sigma_1 [SO_2]_0}{(k_1 + \sigma_2 I)(\sigma_1 - \sigma_3)}$$

The time, t, corresponds to the laser pulse duration of 10 ns.

A similar approach was applied for the three-photon dissociation model shown in Figure 6b. The expressions for the SO^+ and S^+ concentration as a function of laser intensity are

$$[S^+] = k_2 B\left[\left(\frac{1 - e^{-(k_2+k_3)t}}{k_2 + k_3}\right) - \left(\frac{1 - e^{-\sigma_1 It}}{\sigma_1 I}\right)\right]$$

$$[SO^+] = k_3 B\left[\left(\frac{1 - e^{-(k_2+k_3)t}}{k_2 + k_3}\right) - \left(\frac{1 - e^{-\sigma_1 It}}{\sigma_1 I}\right)\right] \quad (3)$$

where

$$B = \frac{\sigma_2 I \sigma_1 I [SO_2]_0}{(k_1 + \sigma_2 I)(\sigma_1 I - k_2 - k_3)}$$

The experimentally observed ion signals from SO^+ and S^+ as a function of the laser intensity are shown in Figure 7. For the three-photon dissociation, eq 3 predicts that the concentrations of SO^+ and S^+ should have the same intensity dependence, in contrast to the experimentally observed dependence of Figure 7. For the two-photon dissociation, on the other hand, eq 2 shows that SO^+ and S^+ should have different intensity dependences. Qualitatively, from the last line of eq 1, it is clear that the slope of a plot of S^+ vs intensity should increase with $[SO^+]$, as shown in the data, where SO^+ increases roughly linearly with I, whereas $[S^+]$ increases as a stronger power. We conclude that the intensity data are consistent with a two-photon dissociation but not with a three-photon dissociation.

4. Conclusions

The multiphoton dissociation process in SO_2 following photoabsorption in the 224−232 nm wavelength region was studied, and possible two-photon versus three-photon dissociation pathways were considered. The total translational energy distributions measured by product imaging techniques strongly suggest a two-photon dissociation pathway, as does the intensity dependence of the SO^+ and S^+ products. The study by Suto et al. indicates that the $\tilde{H}$ Rydberg state in the range 110−115 nm is dissociative, and it seems likely that this Rydberg state is the two-photon intermediate. The role of the intermediate $\tilde{C}$ $^1B_2$ state of SO_2 in this study is to enhance the two-photon transition to the $\tilde{H}$ Rydberg state when the wavelength is coincident with a resonance in the intermediate state, as shown in Figure 1. When the two-photon excitation wavelength is not resonant with the SO_2 $\tilde{C}-\tilde{X}$ transition, direct excitation to $\tilde{H}$ Rydberg state can still be observed as a background in the S^+/SO^+ yield spectra, but this nonresonant two-photon process is considerably weaker.

Product imaging of the $O(^3P_2)$, $S(^1D_2)$, and SO products suggests that following dissociation of SO_2, SO is produced in the A and B electronic states. $S(^1D_2)$ is produced both from two-photon dissociation of SO_2 to give $S(^1D_2) + O_2$ and by single-photon dissociation of SO^+. In the former process, based on energy and momentum conservation and the dissociation threshold for the $S + O_2$ channel (5.9 eV), the maximum energy distributed in O_2 is 3.75 eV, consistent with production of the $S(^1D_2)$ in coincidence with O_2 in the $X\ ^3\Sigma$ (0 eV), $a\ ^1\Delta$ (1 eV) and $b\ ^1\Sigma$ (1.6 eV) electronic states (see Figure 5).

The overall scheme can thus be summarized by the following processes (see also Figure 6a):

$$SO_2(\tilde{X}) \xrightarrow{h\nu} [SO_2\ (\tilde{C}\ ^1B_2)] \xrightarrow{h\nu} SO_2\ (\tilde{H})$$

two-photon absorption

$$SO_2\ (\tilde{H}) \rightarrow SO(A\ ^3\Pi \text{ and } B\ ^3\Sigma^-) + O(^3P) \quad \text{dissociation}$$

$$SO(A\ ^3\Pi \text{ and } B\ ^3\Sigma^-) + h\nu \rightarrow SO^+ + e^- \quad \text{ionization}$$

$$SO^+ + h\nu \rightarrow S^+ + O \quad \text{dissociation}$$

$$\rightarrow S(^1D) + O^+ \quad \text{dissociation}$$

$$SO_2\ (\tilde{H}) \rightarrow S(^1D) + O_2\ (X\ ^3\Sigma, a\ ^1\Delta, \text{and } b\ ^1\Sigma) \quad \text{dissociation}$$

Acknowledgment. This work was supported by the Department of Energy under grant DE-FG02-88ER13934 and, in part, by the National Science Foundation under grant CHE-0239903. Y.L. gratefully acknowledges an NSF EPSCoR Graduate Fellowship.

References and Notes

(1) Yamanouchi, K.; Yamada, H.; Tsuchiya, S. *J. Chem. Phys.* **1988**, *88*, 4664−70.

(2) Katagiri, H.; Sako, T.; Hishikawa, A.; Yazaki, T.; Onda, K.; Yamanouchi, K.; Yoshino, K. *J. Mol. Struct.* **1997**, *413*−*414*, 589−614.

(3) Hansen, N.; Andresen, U.; Dreizler, H.; Grabow, J. U.; Mader, H.; Temps, F. *Chem. Phys. Lett.* **1998**, *289*, 311−318.

(4) Cosofret, B. R.; Dylewski, S. M.; Houston, P. L. *J. Phys. Chem. A* **2000**, *104*, 10240−10246.

(5) Knappenberger, K. L., Jr.; Castleman, A. W., Jr. *J. Phys. Chem. A* **2004**, *108*, 9−14.
(6) Knappenberger, K. L., Jr.; Casteleman, A. W., Jr. *J. Chem. Phys*. **2004**, *121*, 3540−3549.
(7) Golomb, D.; Watanabe, K.; Marmo, F. F. *J. Chem. Phys.* **1962**, *36*, 958−60.
(8) Watkins, I. W. *J. Mol. Spectrosc.* **1969**, *29*, 402−9.
(9) Doktorov, E. V.; Malkin, J. A.; Manko, V. I. *J. Mol. Spectrosc.* **1975**, *56*, 1.
(10) Price, W. C.; Simpson, D. M. *Proc. R. Soc. (London)* **1938**, *A165*, 272−91.
(11) Golomb, D.; Watanabe, K.; Marmo, F. F. *J. Chem. Soc.* **1961**, *36*, 958.
(12) Suto, M.; Day, R. L.; Lee, L. C. *J. Phys. B* **1982**, *15*, 4165−74.
(13) Foo, V. Y.; Brion, C. E.; Hasted, J. B. *Proc. R. Soc., Ser. A* **1971**, *322*, 535−54.
(14) Vuskovic, L.; Trajmar, S. *J. Chem. Phys.* **1982**, *77*, 5436−40.
(15) Avouris, P.; Demuth, J. E.; Schmeisser, D.; Colson, S. D. *J. Chem. Phys.* **1982**, *77*, 1062−3.
(16) Colson, S. D.; Cheung, W. Y.; Glownia, J. H.; Riley, S. J. *Chem. Phys. Lett.* **1980**, *76*, 515.
(17) Zhang, L.; Pei, L.; Dai, J.; Zhang, T.; Chen, C.; Yu, S.; Ma, X. *Chem. Phys. Lett.* **1996**, *259*, 403.
(18) Lalo, C.; Vermeil, C. *J. Photochem.* **1973**, *1*, 321−5.
(19) Lalo, C.; Vermeil, C. *J. Photochem.* **1975**, *3*, 441−54.
(20) Effenhauser, C. S.; Felder, P.; Huber, J. R. *Chem. Phys.* **1990**, *142*, 311−20.
(21) Wilson, M. W.; Rothschild, M.; Muller, D. F.; Rhodes, C. K. *J. Chem. Phys.* **1982**, *77*, 1837−41.
(22) Fotakis, C.; Torre, A.; Donovan, R. J. *J. Photochem.* **1983**, *23*, 97−102.
(23) Wildt, J.; Fink, E. H.; Winter, R.; Zabel, F. *Chem. Phys.* **1983**, *80*, 167−75.
(24) Eppink, A. T. J. B.; Parker, D. H. *Rev. Sci. Instrum.* **1997**, *68*, 3477−3484.
(25) Weiss, M. J.; Hsieh, T.-C.; Meisels, G. G. *J. Chem. Phys.* **1979**, *71*, 567−70.
(26) Dujardin, G.; Leach, S. *J. Chem. Phys.* **1981**, *75*, 2521−31.
(27) Elks, J. M. F.; Western, C. M. *J. Chem. Phys.* **1999**, *110*, 7699−7706.
(28) Archer, C. P.; Elks, J. M. F.; Western, C. M. *J. Chem. Phys.* **2000**, *112*, 6293−6300.
(29) Borin, A. C.; Ornellas, F. R. *Chem. Phys.* **1999**, *247*, 351−364.
(30) Speth, R. S.; Braatz, C.; Tiemann, E. *J. Mol. Spectrosc.* **1998**, *192*, 69−74.
(31) Dibeler, V. H.; Liston, S. K. *J. Chem. Phys.* **1968**, *49*, 482−5.
(32) Sato, T.; Kinugawa, T.; Arikawa, T.; Kawasaki, M. *Chem. Phys.* **1992**, *165*, 173−82.